UFSM

Ciência Florestal

ISSN 1980-5098
OPEN ACCESS

Ci. Fl., Santa Maria, v. 33, n. 2, e71235, p. 1-25, Apr./June 2023 • https://doi.org/10.5902/1980509871235
Submitted: 4th/08/2022 • Approved: 1st/12/2022 • Published: 21st/06/2023

Artigos

Evaluation of polarimetric data and texture attributes in SAR images to discriminate secondary forest in an area of amazon rainforest

Avaliação de dados polarimétricos e de atributos de textura em imagens SAR para discriminar a floresta secundária em uma área de domínio de floresta amazônica

Bárbara Hass Kiyohara[I]
Edson Eyji Sano[II]

[I]Universidade de Brasília, Brasília, DF, Brazil
[II]Embrapa Cerrados, Sobradinho, DF, Brazil

ABSTRACT

This study aims to evaluate the ability of Sentinel-1 polarimetric and backscatter attributes in relation to COSMO-SkyMed (CSM) texture and backscatter features to discriminate secondary vegetation areas in an Amazon Forest domain area, located in Mato Grosso state. In this study, we used polarizations VV and VH from Sentinel-1 Synthetic Aperture Radar (SAR) image and HH from CSM SAR image, both in Single Look Complex format. In the Sentinel-1 image, a covariance matrix was generated and the H-Alpha target decomposition theorem was applied, allowing to obtain the attributes Entropy and Angle alpha. In the CSM image obtained the Gray-Level Co-Occurrence Matrix (GLCM) texture attributes: dissimilarity, contrast, homogeneity and second moment. The Support Vector Machine (SVM) algorithm was used for the classification. The Sentinel-1 polarimetric attributes result, with a Kappa index of 0.70 and an overall accuracy of 79.58%, performed better than those derived from CSM, with a Kappa index of 0.56 and overall accuracy 63.67%. However, the Sentinel-1 and CSM attributes did not present satisfactory results to discriminate the different stages of secondary forest.

Keywords: Amazon; Secondary vegetation; Remote sensing

RESUMO

O objetivo do presente estudo foi avaliar a capacidade de atributos polarimétricos e de retroespalhamento do Sentinel-1 em relação às feições de textura e de retroespalhamento do COSMO-SkyMed (CSM), em discriminar diferentes estágios de floresta secundária em uma área de domínio de Floresta Amazônica, no estado do Mato Grosso. Neste estudo, utilizou-se uma imagem de Radar de Abertura Sintética (SAR) do Sentinel-1 nas polarizações VV e VH e uma imagem SAR do CSM na polarização HH, ambas no formato *Single Look Complex*. Na imagem Sentinel-1 foi gerada a matriz de covariância e aplicado o teorema de decomposição de alvos H-Alpha, para obtenção dos atributos Entropia e Ângulo alfa. Na imagem CSM, foram obtidos os atributos de textura a partir da matriz de co-ocorrência de níveis de cinza (GLCM): dissimilaridade, contraste, homogeneidade e segundo momento. Para a classificação, foi utilizado o algoritmo Máquina de Vetores de Suporte (SVM). A classificação derivada dos atributos polarimétricos do Sentinel-1, com índice Kappa de 0,70 e exatidão global de 79,58%, apresentou desempenho superior àquela derivada do CSM, com índice Kappa de 0,56 e exatidão global de 63,67%. Entretanto, tanto os atributos derivados do Sentinel-1 como do CSM não apresentaram resultados satisfatórios para discriminar os diferentes estágios de floresta secundária.

Palavras-chave: Amazônia; Vegetação secundária; Sensoriamento remoto

1 INTRODUCTION

The Amazon biome has a rich biodiversity, which corresponds to an area with more than 5 million km² of the Brazilian territory (IBGE, 2022). This biome has been suffering significantly from the degradation of actions as deforestation (BERNARD; PENNA; ARAÚJO, 2014; GARRETT; CAMMELLI; FERREIRA; LEVY; VALENTIM; VIEIRA, 2021). However, according to TerraClass Amazon data from 2014, there was an increase of 72.713 km² of secondary vegetation in the Amazon region between 2004 and 2014 years. From the deforested full area in Amazon, 22.8% are in regeneration process (TERRACLASS, 2022). Thus, the secondary vegetation diagnosis after the disturbance is very important for the evaluation of the respective impacts on the ecosystem, such as species diversity, local hydrology, and biomass accumulation rate (KUPLICH, 2006; JAKOVAC; PEÑA-CLAROS; KUYPER; BONGERS, 2015; NOBRE; SAMPAIO; BORMA; CARDOSO, 2016).

Forest regeneration in Brazilian Amazon increased in extent during the 1970s and 1980s and is known to be a net sink of atmospheric CO_2 (KUPLICH; CURRAN;

ATKINSON, 2005; CARVALHO; ADAMI; AMARAL; BEZERRA; AGUIAR, 2019; HEINRICH; DALAGNOL; CASSOL; ROSAN; ALMEIDA; SILVA JUNIOR; CAMPANHARO; HOUSE; SITCH; HALES; ADAMI; ANDERSON; ARAGÃO, 2021). Optical remote sensors are used for the assessment and characterization of the secondary forest stage (LUCAS; HONZÁK; CURRAN; FOODY; MILNE; BROWN; AMARAL, 2000; SOTHE; ALMEIDA; LIESENBERG; SCHIMALSKI, 2017), but frequent cloud cover in the Amazon region often makes it difficult to obtain information based on these sensors. An alternative to this limitation has been the use of active microwave sensors, which include Synthetic Aperture Radar (SAR) (DING; WEN, 2017). The SAR data applications in tropical forests are diverse, and they exploit different sensors, with different polarization options and processing techniques (LI; LU; DUTRA; BATISTELLA, 2012). Sensors that operate at higher wavelengths (L and P bands) allow greater signal penetration in the forest (CARTUS; KELLNDORFER; WALKER; FRANCO; BISHOP; SANTOS; FUENTES, 2014; FURTADO; SILVA; MORAES, 2016), already the shorter microwave sensors (X and C bands) interact more superficially with the canopy structure (KUGLER; SCHULZE; HAJNSEK; PRETZSCH; PAPATHANASSIOU, 2014; TREUHAFT; GONÇALVES; SANTOS; KELLER; PALACE; MADSEN; SULLIVAN; GRAÇA, 2015).

One of the techniques used for forest monitoring is the SAR polarimetric data through of target decomposition theorems (CLOUDE; POTTIER, 1996). This technique allows to identify the scattering mechanism types that occur during the interaction process between electromagnetic microwaves and the target, improving their discrimination (WIEDERKEHR; GAMA; CASTRO; BISPO; BALZTER; SANO; LIESENBERG; SANTOS; MURA, 2020). However, the attributes extracted from the backscatter signal, aggregated with Gray-Level Co-occurrence Matrix (GLCM) texture features (HARALICK; SHANMUGAM; DINSTEIN, 1973) are also used, due to improvement in identification and ability to discriminate different targets, according to the backscattered signal strength from a respective polarization (KUPLICH; CURRAN; ATKINSON, 2005).

The Brazilian Government established several programs to monitor Amazon deforestation using optical data like PRODES (*Programa de Monitoramento do Desflorestamento na Amazônia Legal*) and DETER (*Sistema de Detecção do Desmatamento em Tempo Real*), projects from INPE (*Instituto Nacional de Pesquisas Espaciais*). In 2016, the Censipam (*Centro Gestor e Operacional do Sistema de Proteção da Amazônia*), an agency of the Brazil Ministry of Defense, developed the first program using SAR data. Through the AmazôniaSAR project, Censipam monitors the forest change process in the Brazilian Amazon, with images from the COSMO-SkyMed (CSM) SAR sensor, band X (~ 2.4 - 3.8 cm), in periods of great cloudiness (SIPAM, 2021).

Currently, with the free availability by European Space Agency (ESA), the Sentinel-1A satellite, which operates in the C band (~ 3.9 – 7.5 cm) has become an important tool widely used for forest monitoring (REICHE; HAMUNYELA; VERBESSELT; HOEKMAN; HEROLD, 2018; ESA, 2022). Given this, it is important to develop methodologies that can exploit the potential of this free distribution data to contribute to forest monitoring systems.

Therefore, this study aims to evaluate the potential of attributes derived from polarimetric decomposition and backscatter coefficients of Sentinel-1 double polarization (VV and VH) SAR data in relation to texture and backscatter coefficient attributes of single polarization data from the CSM sensor (HH) to discriminate secondary forest (SF) areas. The research area will be the municipality of Colniza, located in Mato Grosso state.

2 METHODOLOGIES

2.1 Study Area

The study area comprises the eastern portion of Colniza, located in the north of the state of Mato Grosso, between 9˚ 56’ 26.47” and 9˚ 12’ 23.69” of south latitude and between 59˚ 16’ 57” and 59˚ 00’ 52” of west longitude, in an area of approximately

880 km² (Figure 1). The study area comprises a region with the largest deforestation area, imaged by the CSM and Sentinel-1 sensors. The Colniza presented areas that were abandoned after deforestation and are in natural regeneration process now, in different ecological successional stages (IBGE, 2012; MAPBIOMAS, 2022). The vegetation consists of dense and high forests typical of the Amazon, and Cerrado areas, presenting small trees, tortuous, isolated or grouped on a grass-covered. The climate, according to Köppen's classification, is Aw, humid tropical, with a mean temperature of 30°C. The average annual rainfall is 2000 mm (SANTOS, 2010).

Figure 1 – Localization of study area

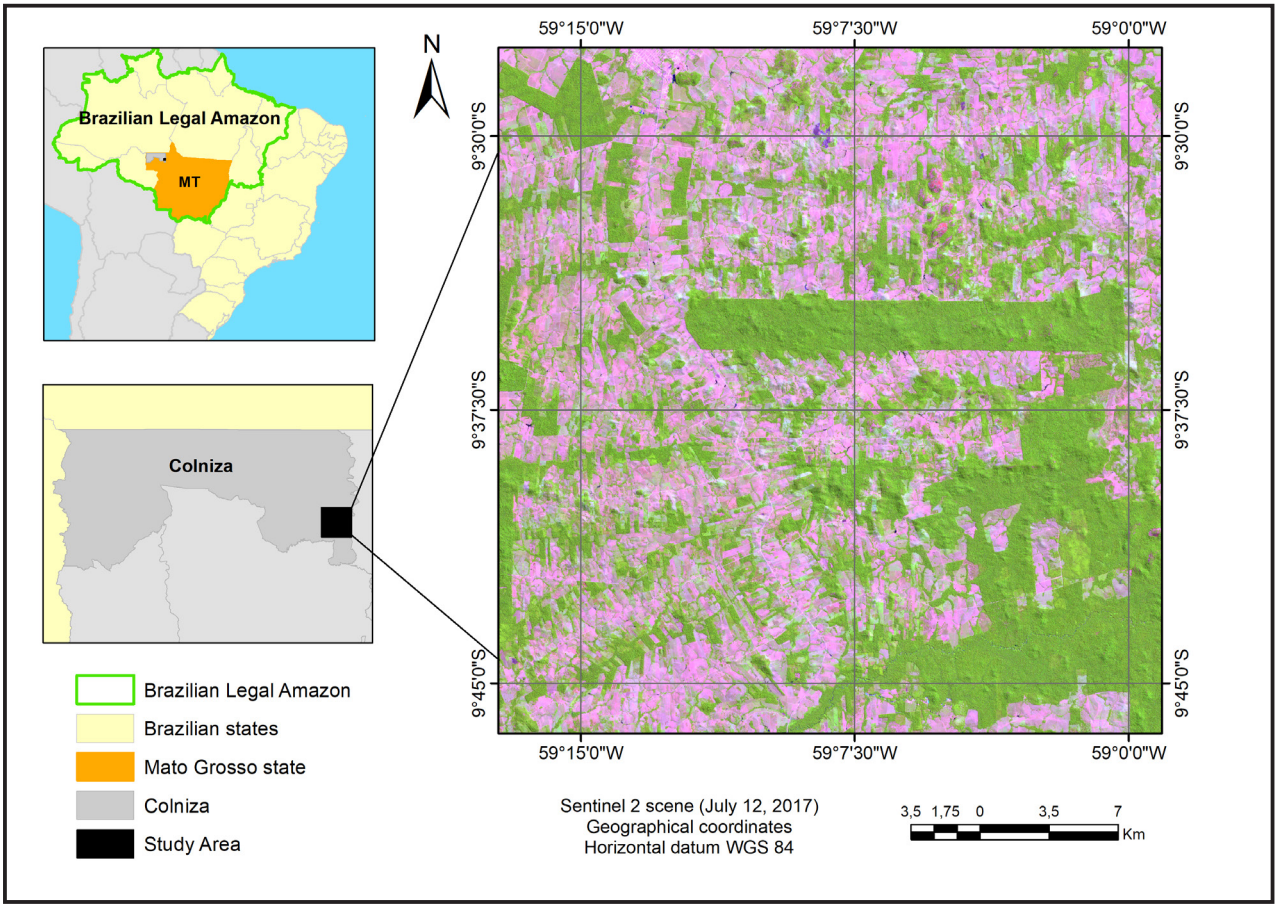

Source: Authors (2022)

In where: The color composite (July 12, 2017) includes the Sentinel 2 bands 11, 8 and 4 in red, green and blue, respectively.

2.2 Radar images processing

The methodological procedures adopted in this study are shown in Figure 2. The Sentinel-1 image used in this study was acquired on September 3, 2017, in IW (Interferometric Wide swath) mode, which has a spatial resolution of 5x20 m, with processing level L1 - Single Look Complex (SLC), being complex images composed by amplitude and phase information, with double polarization: VV and VH. The image was processed in the Sentinel Application Platform 7.0 (SNAP) software. Firstly, the image went through the Terrain Observation with Progressive Scans (TOPSAR) *split* and *orbit* correction process, selecting a smaller subarea to minimize the computational effort. Then, the procedure of TOPSAR *deburst* and radiometric calibration was applied. The Covariance matrix [C2] was generated and resampled by a spatial average *(*Multilook process), a 3x3 pixel window size was performed, with the pixel spacing being converted to 14.05 m in range and azimuth directions.

Figure 2 – Flow diagram of SAR images processing and classification procedures

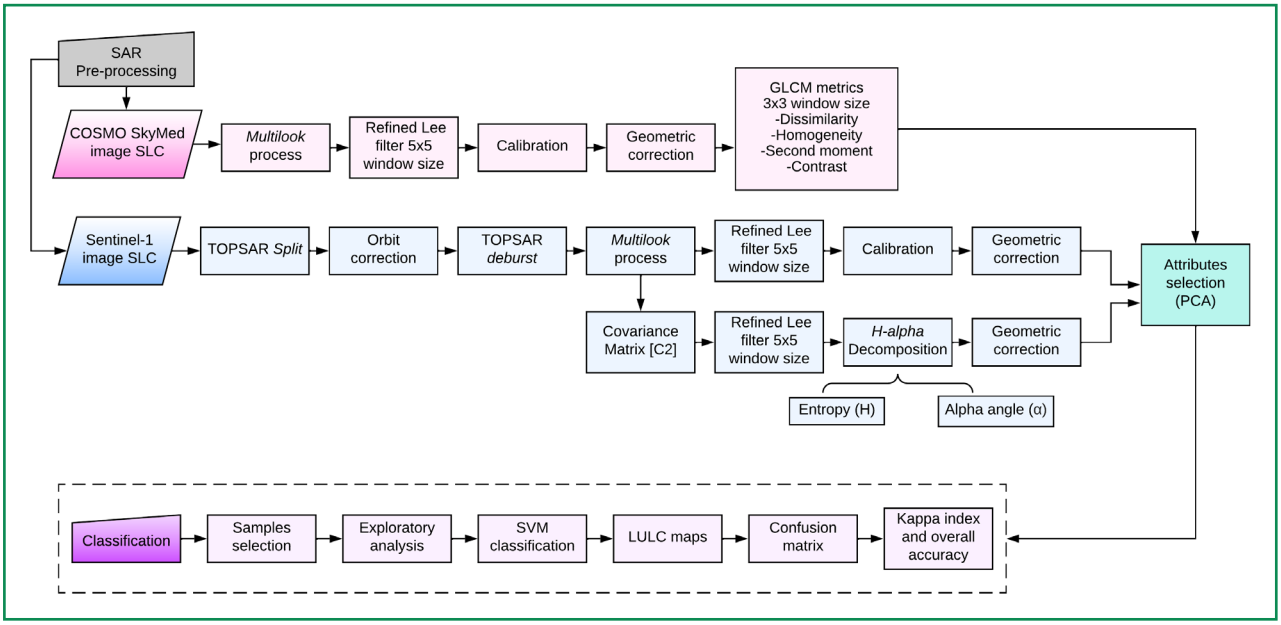

Source: Authors (2022)

To reduce Speckle noise and preserve the details, the Sentinel-1 image was filtered with the Refined Lee filter (LEE; DE GRANDI; DE GRANDI, 1999) with a 5x5 pixel window size. This filter was chosen because it presents good results according to the studies of Pôssa, Gama, Santos, Mura and Bispo (2018) and Wiederkehr, Gama, Castro, Bispo, Balzter, Sano, Liesenberg, Santos and Mura (2020) with polarimetric attributes. After filtering, the backscattering coefficients were obtained in the VV (σVV), VH (σVH), and Cross-polarization ratio (VV/VH) (CPRA). The H-Alpha polarimetric decomposition (CLOUDE; POTTIER, 1997) was performed, extract the attributes of entropy (H) and alpha-angle (α). Finally, the geometric correction of the attributes through geocoding was applied. The last procedure consisted of the attributes geometric correction through geocoding, using the Digital Elevation Model (DEM) Shuttle Radar Topography Mission (SRTM).

The CSM image used in the study was sensed on October 28, 2017, in StripMap mode, sub-mode HIMAGE, in SLC format. The same preprocessing steps were performed to better compare the results of both sensors images. First, the image was calibrated at HH (σHH) polarization, followed by a Multilook process with a 3x3 pixel window size, converting to 3 m spatial resolution in the range and azimuth directions, respectively. Then an image was filtered with the Refined Lee filter, 5x5 pixel window. GLCM was obtained to retrieve various texture metrics from the HH image, with a 3x3 pixel window size (HARALICK; SHANMUGAM; DINSTEIN, 1973). Four texture metrics were computed: Dissimilarity, Homogeneity, Second moment, and Contrast. Previous studies conducted by Kuplich, Curran and Atkinson (2005) and Sothe, Almeida, Liesenberg and Schimalski (2017) showed that homogeneity, contrast, second moment (energy) and dissimilarity were considered the most important ones for identifying vegetation successional stages in a patch of forest, which justifies their use in the present work. All processing steps were performed using Envi 5.5 software and your extension SARscape.

2.3 Attributes selection

The SF samples use in this study were extracted from crossing PRODES deforestation data and areas classified as secondary vegetation of the 2014 TerraClass Amazônia, a project of the National Institute for Space Research (INPE). As PRODES does not contemplate the revisit and reclassification of the mapped areas as deforested, it was possible to identify and vectorize the areas under the regeneration process. These samples were previously validated in *Google Earth Engine* through temporal analysis of the EVI and NDVI indices of the Landsat satellite image catalog.

The selection of the other reference samples representative of the thematic classes was based on the stratified random sampling method using an R11G8B4 color composition of a 10 m resolution Sentinel-2 image dated 12 July 2017, Level 1C geocoded. This composition was chosen because it better identifies the vegetation areas, due the high reflection of vegetation in the near infrared (NIR) region in relation to the marked absorption of chlorophyll in the red region of the electromagnetic spectrum (PONZONI; REZENDE, 2004).

To obtain a samples set with the best representation of each class thematic, the selected samples were well distributed throughout the study area, where 180 polygons were vectorized. We sought to follow a proportion of 75% training samples and 25 % validation samples, respecting the size of each identified class (Table 1) (CONGALTON; GREEN, 2009).

Thus, 9 different land cover types were considered for the classification: Primary Forest (PFO) – Unchanged forests, Advanced Secondary Forest (SF3) - Natural regeneration with over 15 years, Intermediate Secondary Forest (SF2) - Natural regeneration from 5 to 15 years, Initial Secondary Forest (SF1) - Natural regeneration with less than 5 years, Croplands (CRO) - Areas with agriculture cover, Degraded Forest (DEG) – Forest areas with deforestation , Bare Soil (BSO) – Prepared areas to receive the cropland, Pasture (PAS) - Managed pasture areas, with grass cover and Water Bodies (WAT) – Rivers and lakes (Figure 3).

Table 1 – Number of pixel for each class

LULC	Training samples (pixel)	Validation samples (pixel)
PFO	14687	4896
SF1	2083	694
SF2	3796	1265
SF3	4030	1343
CRO	9089	3030
DEG	2026	675
BSO	6785	2262
PAS	5342	1781
WAT	234	78

Source: Authors (2022)

Figure 3 – Samples set of study area. The color composite (July 12, 2017) includes the Sentinel 2 bands 4, 3 and 2 in red, green and blue, respectively

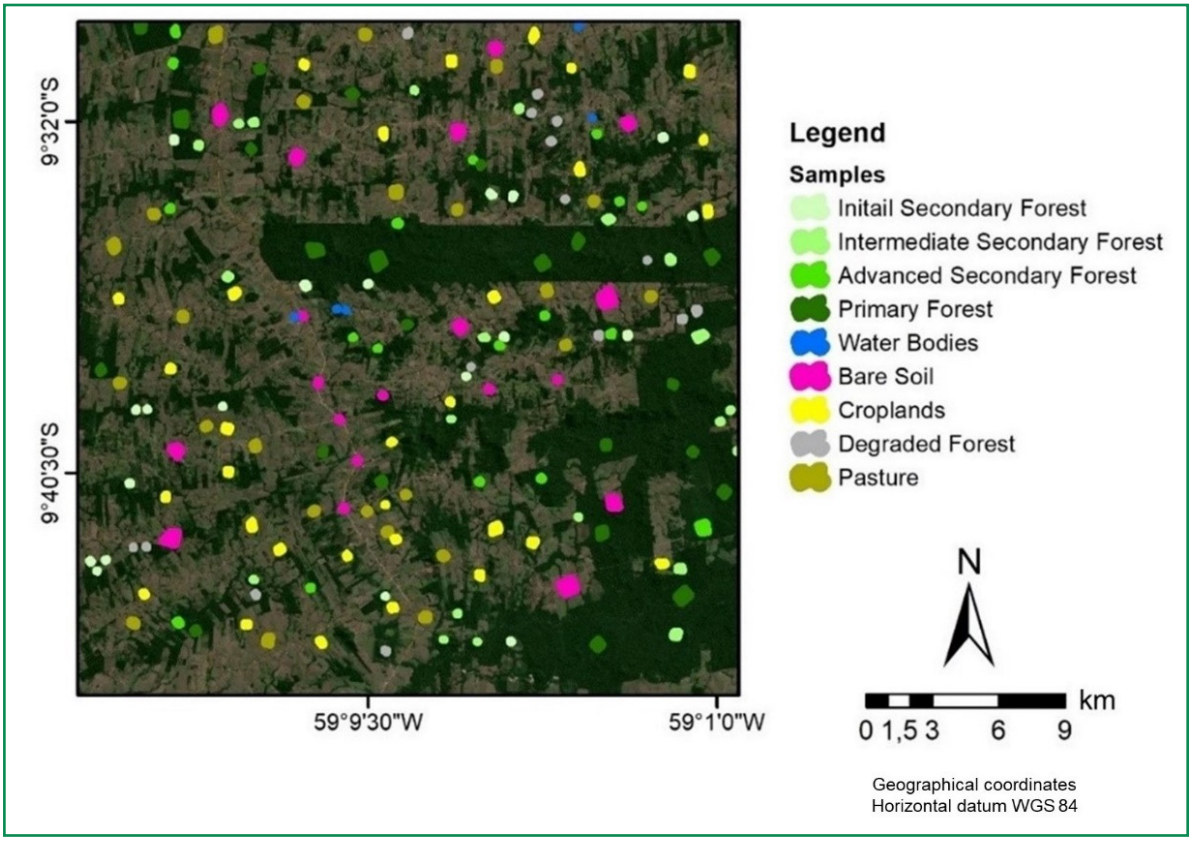

Source: Authors (2022)

An exploratory analysis of attributes derived from polarimetric decomposition, texture, and backscatter metrics was performed to assess the potential for discrimination of SF samples about other thematic classes. Boxplots were made for each attribute from the training samples, considering for the discriminatory understanding of component radiometric information extracted to express the configuration of the different thematic classes. In the attribute selection stage, a Principal Component Analysis (PCA) was performed. The PCA objective is to promote a linear transformation in the data so that the data resulting from this transformation have its most relevant components in the first dimensions (JAFARPOUR; SEDGHI; AMIRANI, 2012).

From the selection of attributes for the secondary vegetation samples, the Land Use and Land Cover (LULC) classification was performed by applying the Support Vector Machine (SVM) classifier. In this work, the radial basis function kernel was chosen, for its superiority in relation to the other functions has been demonstrated in several studies (DURO; FRANKLIN; DUBÉ, 2012; SOTHE; ALMEIDA; LIESENBERG; SCHIMALSKI, 2017). With the classification results and the test samples set, the confusion matrix was generated, to determine the accuracy of the classification that was based on Kappa index and overall accuracy (CONGALTON; GREEN, 2009).

3 RESULTS

3.1 Exploratory analysis of attributes

The exploratory analysis of the Sentinel-1 H-alpha polarimetric decomposition attributes (Figure 4) showed similar values between the different typologies, and some sensitivities could be observed in certain typologies. However, both H and α showed a good ability to discriminate the PFO areas from SF areas in their different stages.

Figure 4 – Boxplots representing the thematic classes distribution over the attributes derived from the H-alpha decomposition

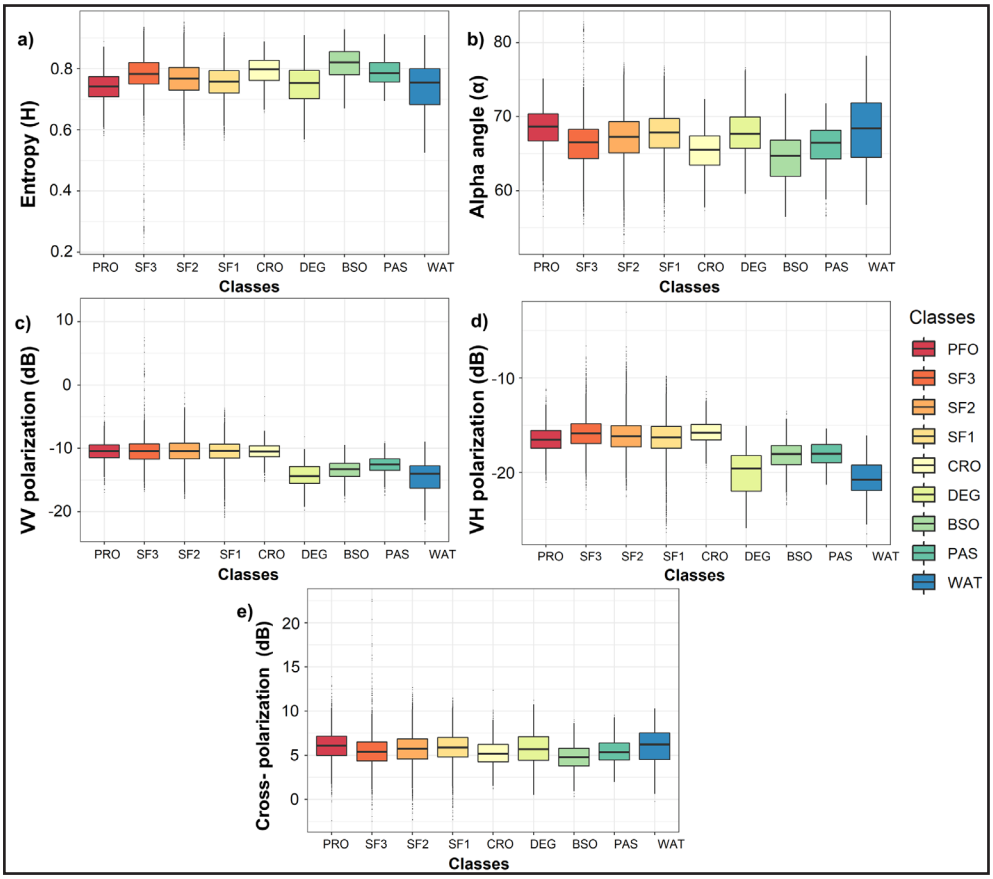

Source: Authors (2022)

In where: entropy H (a); alpha angle α (b); Attributes representing the thematic classes distribution over VV polarization (σVV) (c); VH polarization (σVV) (d); the Cross-polarization ratio (CPRA) (e) attributes derived from backscatter.

The average values of H were relatively lower for the PFO class (H = 0.74), allowing to differentiate it from SF3 (H = 0.79), SF2 (H = 0.77) and SF1 (H = 0.76). Moreover, it is possible to observe that among the different stages of secondary forest, SF3 presented a higher average value of discrimination about SF2 and SF1. The same occurred for the α attribute, but the α scores were relatively higher in the PFO class (α = 68.5 °), with more biomass and complex plant structure compared to SF3 (α = 66.2 °), SF2 (α = 67.1 °), SF1 (α = 67.7 °). The SF3 class presented higher discrimination sensitivity compared to the SF1 and SF2 classes, indicating radiometric similarity between these stages.

The σVH attribute showed greater sensitivity to discriminate most thematic classes. The PFO class presented lower average backscatter values in relation to the SF areas (σVH = -16.5 dB), SF3 (σVH = -15.8 dB), SF2 (σVH = -16.1 dB) and SF1 (σVH = -16.4 dB).

On the other hand, the σVV attribute showed very close average values between the PFO (σVV = -10.5 dB), SF3 (σVV = -10.4 dB), SF2 (σVV = -10.4 dB), SF1 = (σVV = -10.5 dB) classes and CRO (σVV = -10.5 dB), indicating high radiometric similarity for this attribute, and it is not possible to discriminate these respective classes from each other. The CPRA attribute also presented a low discrimination capacity between SF3 (5.41), SF2 (5.73), and SF1 (5.9) classes.

The σHH attribute of the CSM image (Figure 5) exhibited very similar mean backscatter values between the PFO (σHH = -11.7 dB), SF3 (σHH = -11.3 dB), SF2 (σHH = -11.2 dB), SF1 (σHH= -11.2 dB), and CRO (σHH = -11.4 dB) classes.

The Dissimilarity attribute obtained by GLCM texture metrics also showed very similar mean values between PFO, and SF3, 0.203, and 0.209 respectively. This attribute achieved greater discrimination between SF3 class and SF2 class, with fewer biomass classes that presented lower values.

The Second Moment GLCM texture attribute proved high capability to discriminate complex vegetation structure areas from more simple vegetation structures, but failed to discriminate the SF stages from each other.

The Homogeneity GLCM texture attribute had the lowest average values for the PFO class (0.90). The SF classes presented high radiometric similarity among themselves, SF3 (0.92), SF2 (0.93) and SF1 (0.92), and cannot be discriminated according to the regeneration stage by this attribute.

Finally, the Contrast GLCM texture attribute showed very low average values for all thematic classes analyzed, with the median very close to zero. The SF classes presented very high similarity, SF3 (0.007), SF2 (0.005) and SF1 (0.007), and can not be discriminated by this attribute.

Figure 5 – Boxplot representing the thematic classes distribution

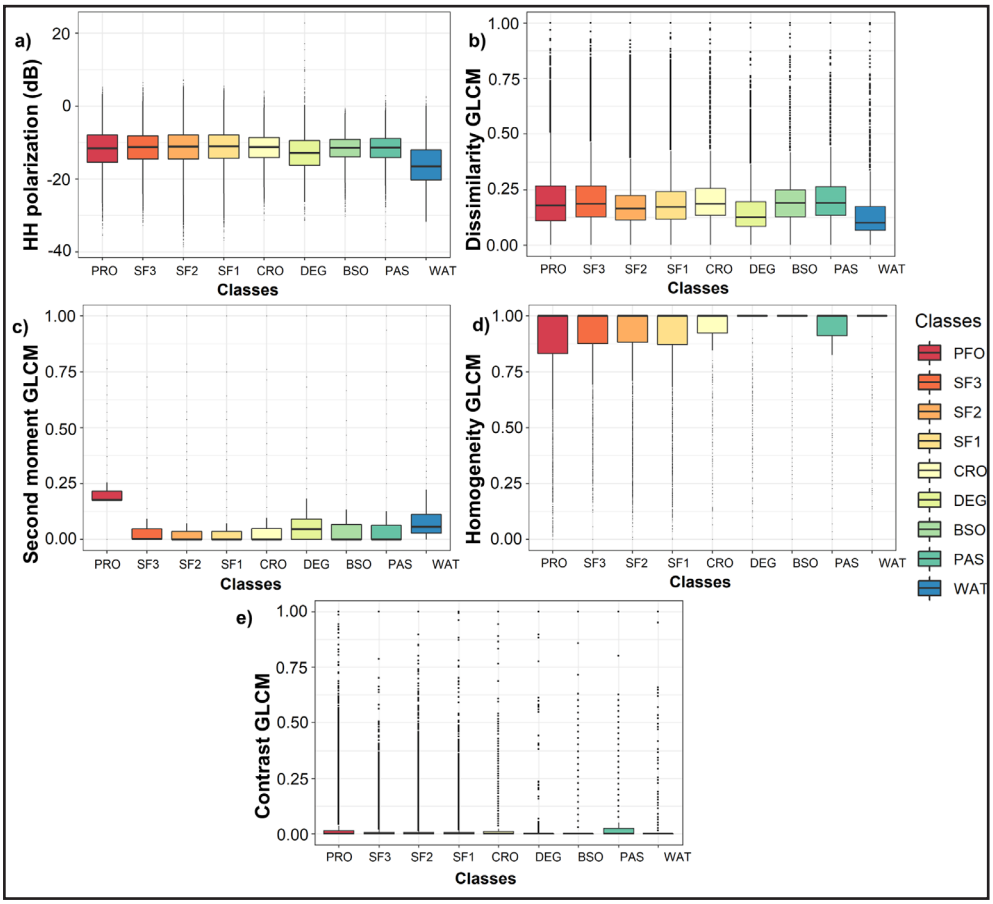

Source: Authors (2022)

In where: HH polarization (σHH) (a); the GLCM texture metrics: Dissimilarity (b), Second moment (c), Homogeneity (d) and Contrast (e).

According to the PCA described in Table 2, it is clear that there is a reduction in variance explained by the first 2 components. From the data derived from Sentinel-1, it can be observed that the first two CP present very close values between the secondary vegetation stages with 71.1% for SF1, 71.7% for SF2, and 72.8% for SF3 of explained variance. Regarding the data derived from the CSM, the values between PC1 and PC2 present a greater difference between the values, whose sum between PC1-2 is 70.9%, 69.9%, and 59.9% for SF1, SF2, and SF3 respectively. Therefore, it is observed that a better grouping between PC1-2.

Table 2 – Percentage of variance explained on each PC [%]

PCA dimensions	PC1			PC2			PC3		
SF classes	SF1	SF2	SF3	SF1	SF2	SF3	SF1	SF2	SF3
Sentinel-1	39.5	38.8	38.7	31.6	32.9	34.1.	27.0	27.0	25.2
CSM	50.9	49.9	39.9	20.0	20.0	20.0	18.4	18.7	19.2

Source: Authors (2022)

Figure 6 shows the polarimetric attributes H and alpha angle from Sentinel-1, presented the largest information in the main components 1-2 (PC1-2). PC1 is simultaneously the direction of the highest variance and the best straight line that minimizes the average distance between values, followed by PC2. Thus, the SVM classification was generated through the combination the attributes H and alpha angle for the Sentinel-1 and GLCM textures homogeneity, dissimilarity and contrast for the CSM image.

Figure 6 – Contribution of each attribute extracted from Sentinel1 and CSM in PC1-2 to SF1 (a), SF2 (b), and SF3 (c) classes

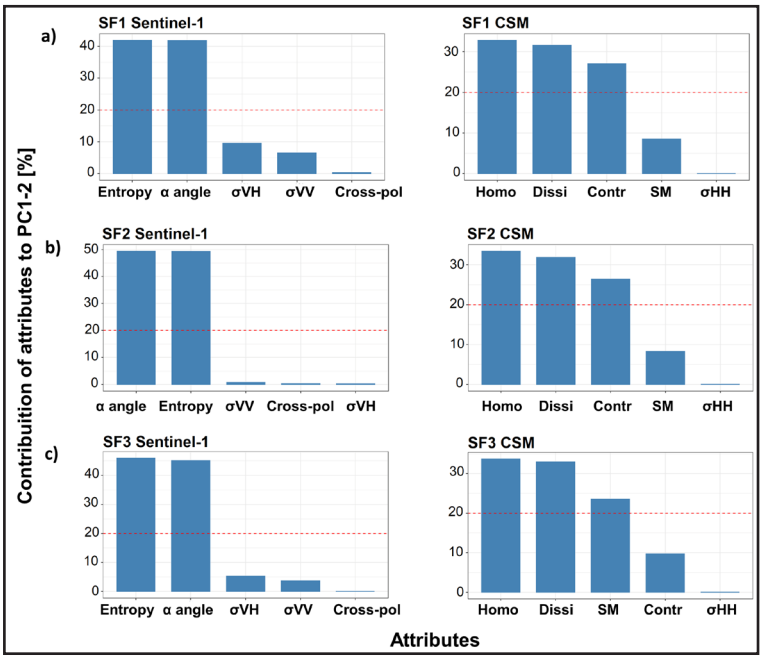

Source: Authors (2022)

In where: Homo: Homogeneity GLCM; Dissi: Dissimilarity GLCM; Contr: ContrastGLCM; SM: Second moment GLCM.

3.2 SVM classification results

The best result was obtained by SVM classification in Sentinel-1-derived polarimetric data, with an overall accuracy of 79.58%. and a Kappa Index of 0.70. This result is considered good according to the scale proposed by Landis and Koch (1977). According to the confusion matrix (Table 3), the classification demonstrated a high ability to discriminate BSO and PFO classes, with an accuracy of 88.35% and 83.13% respectively. Concerning secondary forest areas, the classifier presented a relative high capacity in classifying SF3 areas, with 68.37% producer's accuracy, however, the SF2 and SF1 classes presented lower classification accuracy of 0.12% and 8.25% respectively.

The main classification errors of SF2 and SF1 classes were commissioned for DEG and SF2 classes respectively. About the other classes, the lower classification performance was found for the CRO and DEG classes. The accuracy of the CRO, DEG, BSO, PAS, and WAT classes was 38.15%, 26.81%, 88.35%, 79.43% and 53.02% respectively.

Table 3 – Confusion matrix of the attributes derived from Sentinel 1

		References [%] Overall accuracy: 79.58% - Kappa Index: 0.70									**User's accuracy [%]**
		PFO	SF3	SF2	SF1	CRO	DEG	BSO	PAS	WAT	
Classification [%]	PFO	83.13	7.83	0.06	0.00	0.22	0.00	0.00	0.01	5.36	96.32
	SF3	4.40	68.37	1.76	0.41	9.41	0.07	0.03	4.40	17.37	70.28
	SF2	0.00	0.53	0.12	73.96	8.70	4.29	0.11	3.87	0.15	0.14
	SF1	2.77	14.60	0.87	8.25	42.23	0.12	0.02	4.72	0.38	0.93
	CRO	8.23	2.77	0.03	0.92	38.15	0.00	0.00	0.16	0.09	53.42
	DEG	0.00	0.01	95.92	1.79	0.02	26.81	0.64	0.04	0.00	16.73
	BSO	0.00	0.12	0.03	0.70	0.00	56.3	88.35	7.32	1.01	78.33
	PAS	0.03	5.05	1.17	13.96	1.25	12.33	10.83	79.43	22.6	88.58
	WAT	1.45	0.74	0.03	0.00	0.01	0.05	0.02	0.04	53.02	26.21
Producer's accuracy [%]		83.13	79.43	0.12	8.25	38.15	26.81	88.35	79.43	53.02	

Source: Authors (2022)

The combination of GLCM texture attributes presented an overall accuracy of 63.67%. and a Kappa Index of 0.56, considered as moderate on the scale proposed by Landis and Koch (1977). According to the confusion matrix (Table 4), the classification showed a high capacity to classify the PFO class, with 95% accuracy, however the SF3 and SF2 regeneration classes presented low classification accuracy of 55.37% and 29.37% respectively. However, the SF1 class had the lowest percentage of accuracy about the other classes, with about 1.63%. The main classification errors were commissioned for the PFO and SF3 classes. About other classes, the classification presented a low capacity to discriminate DEG, WAT and CRO, and high capacity to discriminate PAS and BSO. The accuracy of the CRO, DEG, BSO, PAS, and WAT classes was 60.92%, 6.53%, 78.64%, 79.24%, and 45.30%, respectively.

Table 4 – Confusion matrix of the attributes derived from CSM

References [%] Overall accuracy: 63.67% - Kappa Index: 0.56										**User's accuracy [%]**
		PFO	SF3	SF2	SF1	CRO	DEG	BSO	PAS	WAT	
Classification [%]	PFO	94.99	4.69	52.80	26.63	22.14	0.05	0.0	0.08	39.68	68.55
	SF3	4.19	55.37	14.20	37.14	13.92	1.79	0.22	6.83	3.80	41.04
	SF2	0.25	0.44	29.37	0.02	0.02	0.01	0.00	0.01	0.97	96.41
	SF1	0.01	2.67	0.41	1.63	1.49	0.00	0.03	1.86	0.01	12.42
	CRO	0.13	8.86	3.06	32.38	60.92	0.01	0.02	1.43	0.18	51.62
	DEG	0.06	1.12	0.00	0.01	0.02	6.53	7.45	4.10	8.08	14.83
	BSO	0.04	0.33	0.00	0.01	0.01	73.14	78.64	6.34	0.73	61.47
	PAS	0.11	25.86	0.14	2.16	1.47	17.71	13.61	79.24	1.24	78.27
	WAT	0.22	0.67	0.00	0.00	0.01	0.75	0.02	0.11	45.30	49.29
Producer's accuracy [%]		94.99	55.37	29.37	1.63	60.92	6.53	78.64	79.24	45.30	

Source: Authors (2022)

Figure 7 shows the potential of the Sentinel-1 H-alpha decomposition attribute group and CSM-derived GLCM texture attributes to produce LULC maps from the SVM classifier.

Figure 7 – SVM classification results

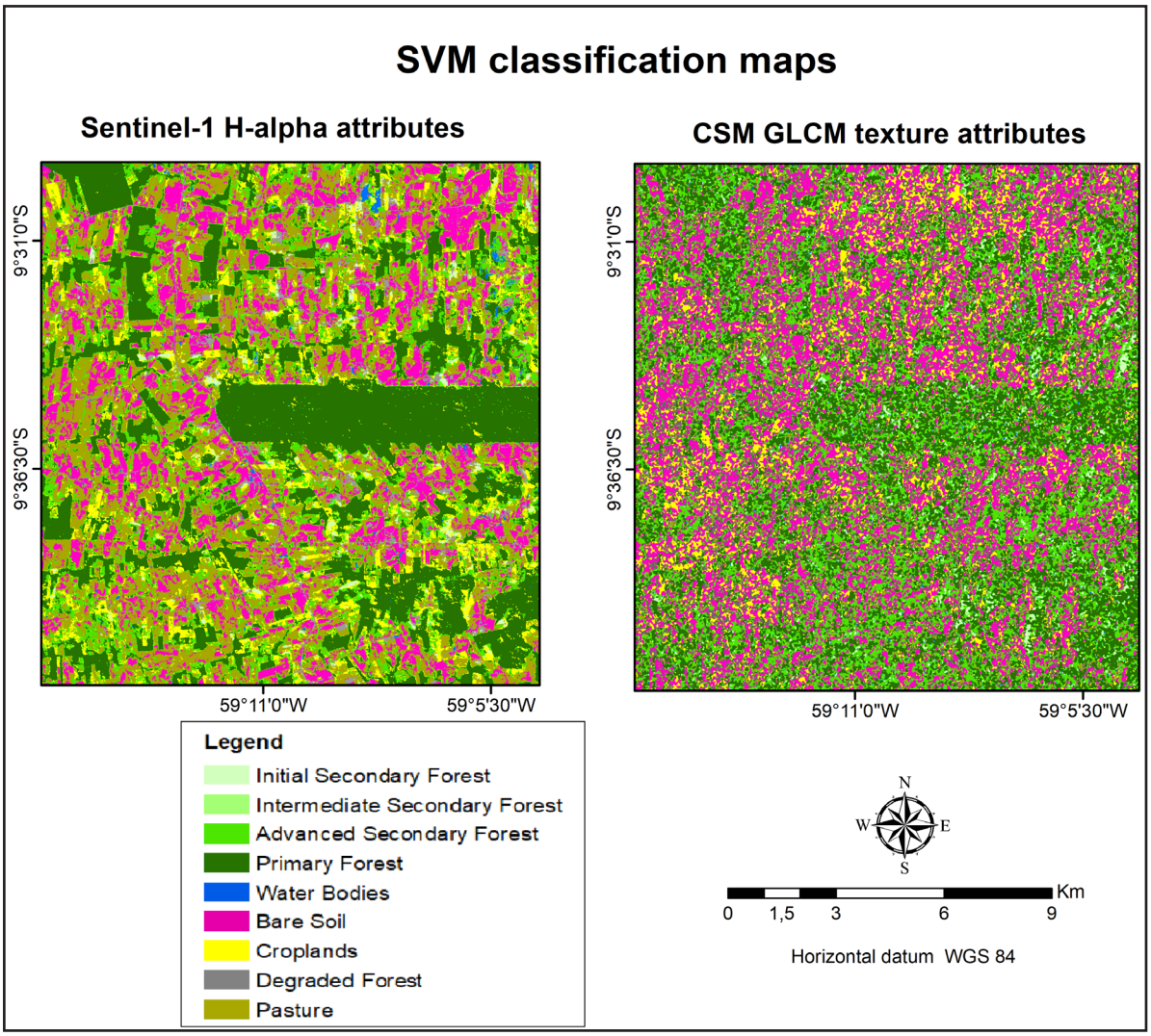

Source: Authors (2022)

We note a predominance of PFO and BSO classes in the the study area. The SF classes occupy less than 15% of the study area from Sentinel-1 attributes and are distributed throughout the study area in relatively small areas. However, in the classification derived from the CSM attributes, the SF classes represent 37% of the total area, distributed together with the PFO class. The classes DEG and WAT are the smallest classes in the study area, in both classification maps (Table 5).

Table 5 – LULC areas derived from SVM classification results (km²).

LULC	Sentinel-1	CSM
PFO	294.5	196.1
SF1	29.3	79.2
SF2	31.4	69.5
SF3	66.6	176.7
CRO	166.7	78.9
DEG	27.6	21.1
BSO	182.6	244.3
PAS	96.5	14.2
WAT	5.4	0.6

Source: Authors (2022)

4 DISCUSSION

Attributes derived from Sentinel-1 H-alpha polarimetric decomposition technique showed good discrimination potential for the SF3 class. However, the potential to distinguish SF1 and SF2 classes was not good. The H attribute presented high average values for the forest classes in different successional stages, indicating that the different scattering mechanisms contributed similarly to the signal returned to the sensor, only distinguishing the SF3 class from the other SF classes, according to SVM classification results.

According to exploratory analyzes using boxplot and PCA, the attributes extracted from the Sentinel-1 H-alpha decomposition exhibited the better capacity to discriminate secondary forest classes from other classes than from backscatter coefficients, however, the values are still similar. Entropy measures the degree of random distribution of backscatter mechanisms and the alpha angle makes it possible to identify and describe the type of target backscatter mechanism (CLOUDE; POTTIER, 1996).

About the analysis of GLCM texture attributes from CSM, the discrimination between regeneration areas was low. The values of the classes are directly related to the types of canopies structured in the different regeneration stages. The canopy

of the initial and intermediate succession stages is usually smaller in size and density than those in the more advanced stage of secondary forest. The PFO and SF3 classes presented a higher general discrimination capacity than the other classes with lower vegetation cover. However, despite the pre-processing filtering, the CSM image presented a grainy appearance (speckle effect) that difficult the interpretation and classification. This effect is magnified due to the short wavelength of the X-band (KUCK; GOMEZ; SANO; BISPO; HONÓRIO, 2021).

The Confusion Matrix of Table 4 shows the low classificatory performance of the different successional stage classes derived from the CSM GLCM texture attributes. The X band has more interaction with the top of the canopy than the C-band, without a wide range of target penetration, detects the still conserved structures, although they may be degraded by burns, for example, thus generating a spectral confusion between them classes (AZEVEDO; SANTOS; GAMA; GRAÇA; MURA, 2014).

Azevedo, Santos, Gama, Graça and Mura (2014) in their study on LULC of an area in the Amazon with CSM data concluded that the inclusion of textural information did not indicate significant improvement in thematic performance, being statistically similar to that achieved by the group of attributes formed only by the intensity images. The authors suggest that the use of L-band data associated with X-band data allows the aggregation of information from backscattering of structures located inside the canopy, or even soil information, better characterizing the plant typology present in the study area.

Wiederkehr, Gama, Castro, Bispo, Balzter, Sano, Liesenberg, Santos and Mura (2020) used polarimetric decomposition techniques in ALOS PALSAR-2 L band images for LULC classification in the Tapajos Forest. In this study, the best attributes for discrimination secondary vegetation classes were anisotropy, derived from the decomposition Cloude Pottier, and volumetric scattering derived from the Freeman-Durden decomposition. Li, Lu, Dutra and Batistella (2012) analyzed data from the ALOS PALSAR-1 L band and RADARSAT C band for LULC classification in Altamira, Pará,

Brazil, through the combination of radiometric and textural images. The authors claim that L-band data provided a much better classification than C-band data. However, neither L-band or C-band data can accurately separate detailed forest. L-band data provided reasonably good classification accuracies for a set of classes such as forest and secondary succession.

In this study, the attributes derived from Sentinel-1 and CSM were not able to discriminate the different stages of secondary forest. According to Pereira, Freitas, Sant'anna and Reis (2016), one factor that can contribute to these results is the high complexity of forest cover presented by these classes. Because of this complexity, differences in vegetation structure cannot be evident, mainly regarding classes of sequential stages of regrowth.

Future research suggests exploring L-band SAR data with different polarimetric decompositions to discriminate areas of secondary vegetation. Additionally, it is suggested to perform tests with interferometry techniques, as it provides additional information on the three-dimensional structure of the targets in the image. This technique has already been employed in large-scale mapping and forest monitoring, as it increases the classification accuracy (GAMA; MURA; ALBUQUERQUE; SANTOS, 2010).

5 CONCLUSIONS

This study shows the difficulties presented by working with SAR data and secondary forest different stages. C-band data provided reasonably good classification accuracies for a coarse set of classes such as primary forest, secondary forest advanced, with overall accuracy and kappa coefficient of 72.2% and 0.64, respectively. The attributes derived from the H-Alpha polarimetric decomposition present better capacity to discriminate secondary forest classes from other classes, however, the values are still similar, it is not possible to discriminate the classes of secondary vegetation from each other.

However, X-band provided overall accuracy and kappa coefficient of only 63.67% and 0.56 for the SVM classification. According to the analysis of boxplots and PCA, the attributes extracted by the backscattering coefficients in the VV and VH polarizations of Sentinel-1 and the HH polarization of CSM sensor in the proposed LULC classification did not show good results for the SF classes discrimination.

PCA was used in this study to reduce the dimensions of the original variables without loss of information by summarizing the data containing many variables by a smaller set of variables. Given the results obtained, the PCA proved to be effective, allowing the removal or disposal of three attributes derived from Sentinel-1 backscattering and two attributes related to GLCM texture and backscattering, attributes that showed low variability or were redundant because they correlated with one another. Those of major importance to the main components in the 1st and 2nd dimensions. Thus, fewer attributes were required to explain the overall variation, resulting in time and resource savings.

Preliminary results from this study suggest that Sentinel-1 IW data may be an important source of information for the mapping of land cover in the domain of tropical forests, as they can properly distinguish between those of primary structural and physiognomic configuration. The advanced successional phase of the other typological features of the vegetation cover, as well as exposed soil and cultivated area. The results presented in this research hoping to improve LULC mapping with the use of X-band and C-band data. It is suggested the association of SAR interferometry could contribute to the discrimination of forest classes with the use of interferometric coherence and even with altimetric information. Also, as future research it is suggested to explore L-band SAR data with different polarimetric decompositions techniques.

ACKNOWLEDGEMENTS

The authors acknowledgment Telespazio which provided COSMO Sky-Med data and Censipan (Centro Gestor e Operacional do Sistema de Proteção da Amazônia -

Brazil Ministry of Defense) for the structure and support in this project. This research was supported by the Coordenação de Aperfeiçoamento de Pessoal de Nível Superior (CAPES, Process # 88887.500593/2020-00) and the Conselho Nacional de Desenvolvimento Científico e Tecnológico (CNPq, Process # 380070/2020-0).

REFERENCES

AZEVEDO, A. R. de; SANTOS, J. R. dos; GAMA, F. F.; GRAÇA, P. M. L. de A.; MURA, J. C. Caracterização de uso e cobertura da terra na Amazônia utilizando imagens duais multitemporais do COSMO-SkyMed. **Acta Amazonica**, v. 44, n. 1, p. 87- 98, 2014.

BERNARD, E.; PENNA, L. A.; ARAÚJO, E. Downgrading, downsizing, gazettement, and reclassification of protected areas in Brazil. **Conservation Biology**, v. 28, n. 4, p. 939-950, 2014.

CARTUS, O.; KELLNDORFER, J.; WALKER, W.; FRANCO, C.; BISHOP, J.; SANTOS, L.; FUENTES, J. M. M. A national, detailed map of forest aboveground carbon stocks in Mexico. **Remote Sensing**, v. 6, n. 6, p. 5559-5588, 2014.

CARVALHO, R.; ADAMI, M.; AMARAL, S.; BEZERRA, F. G.; AGUIAR, A. P. D. de. Changes in secondary vegetation dynamics in a context of decreasing deforestation rates in Pará, Brazilian Amazon. **Applied Geography**, v. 106, p. 40-49, 2019.

CONGALTON, R. G.; GREEN, K. **Assessing the accuracy of remotely sensed data:** principles and practices. 2.ed. New York: Lewis Publishers, 183 pp., 2009.

CLOUDE, S. R.; POTTIER, E. A review of target decomposition theorems in radar polarimetry. **IEEE transactions on geoscience and remote sensing**, v. 34, n. 2, p. 498-518, 1996.

CLOUDE, S. R.; POTTIER, E. An entropy-based classification scheme for land application of polarimetric SAR. **IEEE Transactions on Geoscience and Remote Sensing**, v. 35, n.1, p. 68-78, 1997.

DING, B.; WEN, G. Exploiting multi-view SAR images for robust target recognition. **Remote Sensing**, v. 9, n. 11, p.1150, 2017.

DURO, D. C.; FRANKLIN, S. E.; DUBÉ, M. G. A comparison of pixel-based and object-based image analysis with selected machine learning algorithms for the classification of agricultural landscapes using SPOT-5 HRG imagery. **Remote Sensing of Environment**, v. 118, p. 259-272, 2012.

ESA. European Space Agency. **Copernicus Sentinel-1**: The SAR imaging constellation for land and ocean services, 2019. Available at: https://earth.esa.int/web/eoportal/satellite-missions/c-missions/copernicus-sentinel-1. Access in: 10 September 2019.

FURTADO, L. F. A.; SILVA, T. S. F.; MORAES, E. M. L. M. Dual-season and full-polarimetric C band SAR assessment for vegetation mapping in the Amazon varzea wetlands. **Remote Sensing of Environment**, v. 174, p. 212-222, 2016.

GAMA, F. F.; MURA, J. C.; ALBUQUERQUE, P. C. G. de; SANTOS, J. R. dos. Avaliação do potencial da interferometria sar para o mapeamento altimétrico de áreas reflorestadas por eucalyptus sp. **Boletim de Ciências Geodésicas**, v. 16, n.4, p. 519-537, 2010.

GARRETT, R. D.; CAMMELLI, F.; FERREIRA, J.; LEVY, S. A.; VALENTIM, J.; VIEIRA, I. Forests and Sustainable Development in the Brazilian Amazon: History, Trends, and Future Prospects. **Annual Review of Environment and Resources**, v. 46, p. 625-652, 2021.

HARALICK, R. M.; SHANMUGAM, K.; DINSTEIN, I. Textural features for image classification. **IEEE Transactions on Systems, Man and Cybernetics**, v. 6, p. 610-621, 1973.

HEINRICH, V. H. A.; DALAGNOL, R.; CASSOL, H. L. G.; ROSAN, T. M.; ALMEIDA, C. T. de; SILVA JUNIOR, C. H. L.; CAMPANHARO, W. A.; HOUSE, J. I.; SITCH, S.; HALES, T. C.; ADAMI, M.; ANDERSON, L. O.; ARAGÃO, L. E. O. C. Large carbon sink potential of secondary forests in the Brazilian Amazon to mitigate climate change. **Nature Communications**, v. 12, p. 1-11, 2021.

IBGE. Amazônia Legal. Available at: https://www.ibge.gov.br/geociencias/cartas-e-mapas/mapas-regionais/15819-amazonia-legal.html?=&t=acesso-ao-produto. Access in: 12 September 2022.

IBGE. **Manual Técnico da Vegetação Brasileira. Manuais Técnicos em Geociências**, n. 1, Rio de Janeiro, IBGE, 274 p, 2012.

JAFARPOUR, S.; SEDGHI, Z.; AMIRANI, M. C. A robust brain MRI classification with GLCM features. **International Journal of Computer Applications**, v. 37, n.12, p. 1-5, 2012.

JAKOVAC, C. C.; PEÑA-CLAROS, M.; KUYPER, T. W.; BONGERS, F. Loss of secondary-forest resilience by land-use intensification in the Amazon. **Journal of Ecology**, v. 103, n.1, p. 67-77, 2015.

KUCK, T. N.; GOMEZ, L. D.; SANO, E. E.; BISPO, P. D. C.; HONÓRIO, D. D. Performance of Speckle Filters for COSMO-SkyMed Images from the Brazilian Amazon. **IEEE Geoscience and Remote Sensing Letters**, v. 19, p. 1-5, 2021.

KUGLER, F.; SCHULZE, D.; HAJNSEK, I.; PRETZSCH, H.; PAPATHANASSIOU, K. P. TanDEM-X Pol-InSAR performance for forest height estimation. **IEEE Transactions on Geoscience and Remote Sensing**, v. 52, n.10, p. 6404-6422, 2014.

KUPLICH, T. M. Classifying regenerating forest stages in Amazonia using remotely sensed images and a neural network. **Forest Ecology and Management**, v. 234, n.1-3, p. 1-9, 2006.

KUPLICH, T. M.; CURRAN, P. J.; ATKINSON, P. M. Relating SAR image texture to the biomass of regenerating tropical forests. **International Journal of Remote Sensing**, v. 26, n.21, p. 4829-4854, 2005.

LANDIS, J. R.; KOCH, G. G. The measurement of observer agreement for categorical data. **Biometrics**, v. 33, p. 159-174, 1977.

LEE, R.; DE GRANDI, M. R.; DE GRANDI, G. Polarimetric SAR speckle filtering and its implication for classification. **IEEE Transactions on Geoscience and Remote Sensing**, v. 37, v. 5, p. 2363-2373, 1999.

LI, G.; LU, D.; DUTRA, L.; BATISTELLA, M. A comparative analysis of ALOS PALSAR L-band and RADARSAT-2 C-band data for land-cover classification in a tropical moist region. **ISPRS Journal of Photogrammetry and Remote Sensing**, v. 70, p. 26-38, 2012.

LUCAS, R. M.; HONZÁK, M.; CURRAN, P. J.; FOODY, G. M.; MILNE, R.; BROWN, T.; AMARAL, S. Mapping the regional extent of tropical forest regeneration stages in the Brazilian Legal Amazon using NOAA AVHRR data. **International Journal of Remote Sensing**, v. 21, n. 15, p. 2855-2881, 2000.

MAPBIOMAS. MapBiomas v. 6.0. Available at: https://mapbiomas.org/en/statistics. Access in: 25 June 2022.

NOBRE, C. A.; SAMPAIO, G.; BORMA, L. S.; CARDOSO, M. Land-use and climate change risks in the Amazon and the need of a novel sustainable development paradigm. **Proceedings of the National Academy of Sciences**, v. 113, n. 39, p. 10759-10768, 2016.

PEREIRA, L. O.; FREITAS, C. C.; SANT'ANNA, S. J. S.; REIS, M. S. ALOS/PALSAR data evaluation for land use and land cover mapping in the Amazon region. **IEEE Journal of Selected Topics in Applied Earth Observations and Remote Sensing**, v. 9, n. 12, p. 5413-5423, 2016.

PONZONI, F. J.; REZENDE, A. N. P. Caracterização espectral de estágios sucessionais de vegetação secundária arbórea em Altamira (PA), através de dados orbitais. **Revista Árvore**, v. 28, p. 535–545, 2004.

PÔSSA, E. M.; GAMA, F. F.; SANTOS, J. R. dos; MURA, J. C.; BISPO, P. da C. Análise de uso e cobertura da terra na região do tapajós, Amazônia central, a partir de dado polarimétrico PALSAR/ALOS-1 e coerência interferométrica TanDEM-X. **Revista Brasileira de Geografia Física**, v. 11, n. 6, p. 2094-2108, 2018.

REICHE, J.; HAMUNYELA, E.; VERBESSELT, J.; HOEKMAN, D.; HEROLD, M. Improving near-real time deforestation monitoring in tropical dry forests by combining dense Sentinel-1 time series with Landsat and ALOS-2 PALSAR-2. **Remote Sensing of Environment**, v. 204, p. 147-161, 2018.

SANTOS, M.V. **Zoneamento Sócio-Econômico-Ecológico:** diagnóstico sócio-econômico-ecológico do Estado de Mato Grosso e assistência técnica na formulação da 2ª aproximação. Cuiabá, MT: SEPLAN-MT, 2000.

SIPAM. Projeto Amazônia SAR: desenvolvimento operacional e primeiros resultados na identificação do desmatamento com Radar orbital. Available at: http://www.sipam.gov.br/projeto-amazonia-sar. Access in: 21 September 2021.

SOTHE, C.; ALMEIDA, C. M. de; LIESENBERG, V.; SCHIMALSKI, M. B. Evaluating Sentinel-2 and Landsat-8 Data to Map Successional Forest Stages in a Subtropical Forest in Southern Brazil, **Remote Sensing**, v. 9, n. 8, p. 838, 2017.

TERRACLASS. Amazonia Legal. Available at: https://www.terraclass.gov.br/geoportal-aml/ Access: 3 February 2022.

TREUHAFT, R.; GONÇALVES, F.; SANTOS, J. R. dos; KELLER, M.; PALACE, M.; MADSEN, S. N.; SULLIVAN, F.; GRAÇA, P. M. L. A. Tropical-forest biomass estimation at X-band from the spaceborne TanDEM-X interferometer. **IEEE Geoscience and Remote Sensing Letters**, v. 12, n. 2, p. 239-243, 2015.

WIEDERKEHR, N. C.; GAMA, F. F.; CASTRO, P. B. N.; BISPO, P. da C.; BALZTER, H.; SANO, E. E.; LIESENBERG, V.; SANTOS, J. R.; MURA, J. C. Discriminating Forest successional stages, forest degradation, and land use in central amazon using ALOS/PALSAR-2 full-polarimetric data. **Remote Sensing**, v.12, p. 3512, 2020.

Authorship Contribution

1 Bárbara Hass Kiyohara

Manager and Environmental Analyst, PhD in Applied Geosciences and Geodynamics

https://orcid.org/0000-0003-3402-5604 • babs.hass@gmail.com

Contribution: Conceptualization; Data curation; Formal analysis; Funding acquisition; Investigation; Software; Visualization; Writing – original draft

2 Edson Eyji Sano

Geologist, Professor, Researcher, PhD in Soil Science

https://orcid.org/0000-0001-5760-556X • edson.sano@embrapa.br

Contribution: Methodology; Project administration; Resources; Supervision; Validation; Writing – review & editing

How to quote this article

Kiyohara, B. H.; Sano, E. E. Evaluation of polarimetric data and texture attributes in sar images to discriminate secondary forest in an area of amazon rainforest. Ciência Florestal, Santa Maria, v. 33, n. 2, e71235, p. 1-25, 2023. DOI 10.5902/1980509871235. Available from: https://doi.org/10.5902/1980509871235.